



HAL
open science

Parametric Validation of the Reservoir-Computing-Based Machine Learning Algorithm Applied to Lorenz System Reconstructed Dynamics

Samuele Mazzi, David Zarzoso

► **To cite this version:**

Samuele Mazzi, David Zarzoso. Parametric Validation of the Reservoir-Computing-Based Machine Learning Algorithm Applied to Lorenz System Reconstructed Dynamics. *Complex Systems*, In press. hal-03200715v1

HAL Id: hal-03200715

<https://hal.science/hal-03200715v1>

Submitted on 16 Apr 2021 (v1), last revised 8 Feb 2022 (v2)

HAL is a multi-disciplinary open access archive for the deposit and dissemination of scientific research documents, whether they are published or not. The documents may come from teaching and research institutions in France or abroad, or from public or private research centers.

L'archive ouverte pluridisciplinaire **HAL**, est destinée au dépôt et à la diffusion de documents scientifiques de niveau recherche, publiés ou non, émanant des établissements d'enseignement et de recherche français ou étrangers, des laboratoires publics ou privés.

Parametric Validation of the Reservoir-Computing-Based Machine Learning Algorithm to Predict Chaotic Trajectories

Samuele Mazzi^{a,b} and David Zarzoso^a

^a Aix-Marseille Université, CNRS, PIIM, UMR 7345 Marseille, France

^b CEA, IRFM, F-13108 Saint-Paul-lez-Durance, France

A detailed parametric analysis is presented, where the recent method based on the Reservoir Computing paradigm, including its statistical robustness, is studied. It is observed that the prediction capabilities of the Reservoir Computing approach strongly depend on the random initialisation of both the input and the reservoir layers. Special emphasis is put on finding the region in the hyperparameter space where the ensemble-averaged training and generalization errors together with their variance are minimized. The statistical analysis presented here is based on the Projection on Proper Elements (PoPe) method [T. Cartier-Michaud *et al.*, Phys. Plasmas **23**, 020702 (2016)].

I. INTRODUCTION

A chaotic system is defined as that for which its time evolution is extremely sensitive to the initial conditions. In that sense, given two initial conditions arbitrarily close, the distance between the respective time evolution of the system diverges exponentially. The existence and analysis of chaotic systems is of prime importance, for chaos is everywhere in our Universe. Chaotic systems are found in social relations, in financial markets, in the atmosphere and in the motion of planets, for instance. Independently of the mathematical challenge of analysing the time evolution of chaotic systems, chaos plays a crucial role worldwide and can lead to catastrophic consequences, for it is theoretically unpredictable. Therefore, understanding, predicting and eventually controlling chaos might open new ways to optimise and ameliorate our daily lives. In this paper, we present how chaotic trajectories can be predicted using Machine Learning (ML) techniques. For this purpose, we start and base our study upon a well-known chaotic system: the Lorenz system [1], which is given by the equations:

$$\begin{cases} \dot{x} = F_x(x, y, z; a) = a(y - x) & (1a) \\ \dot{y} = F_y(x, y, z; b) = x(b - z) - y & (1b) \\ \dot{z} = F_z(x, y, z; c) = xy - cz & (1c) \end{cases}$$

These equations were derived for the first time by Lorenz, after simplifying a set of partial differential equations describing the motion of a fluid in between two layers of the atmosphere. Therefore, the parameters a , b and c have a real physical meaning, especially b , which correspond to the convection rate. Lorenz, in his seminal paper, used the values $a = 10$, $b = 28$ and $c = 8/3$. It was shown that those values correspond to a chaotic regime, leading to the famous Lorenz butterfly. Nevertheless, it was later shown that the system can exhibit different regimes, depending on the parameter b . In this Letter, we start using this model with the same aforementioned parameters in order to illustrate our results. We will later analyse the impact of the choice of these parameters on the prediction of the trajectories. Such a

system was very recently analysed in a couple of publications [2, 3], where the chaotic trajectories of the Lorenz system were predicted using the so-called Reservoir Computing (RC) ML approach [4]. Also, the same approach was employed to infer unmeasured variables in model-free chaotic systems [5]. The difference between the prediction and the inference methodology comes from the nature of the input signal. Whereas for prediction the input signal is nothing else but the signal predicted in the previous time step and therefore directly related to the output of the Artificial Intelligence System (AIS), for inference purposes the input signal is not related to the output of the AIS, but comes from a given set of measured variables. In essence, it is intuitive to think that using an AIS for prediction is less stable than using it for inference, since the error in the prediction can be amplified as it is re-introduced in the system in the next time step.

The AIS method here employed takes inspiration from the paradigm of the reservoir computers, which were developed in two independent studies of the early current century [6, 7]. Due to the difficulty of designing efficient recurrent neural network (RNN) architectures and the subsequent inaccuracy of simplistic RNNs [8], Jaeger and Maass proposed the approach of the reservoir computing, which differs from the standard RNN in being essentially split into two levels. The internal layer is composed by the so-called *reservoir*, which is a randomly initialised RNN. Indeed, the output level, usually called *readout*, is a feed-forward layer which realizes an optimized output function in order to obtain the predicted vector. In the case of the RC proposed by Jaeger, the Echo State Network (ESN) [4, 6, 9], and also in the present study the output function is a linear regression. Thus, the weights of the connected nodes of the *reservoir* are fixed randomly, whereas the dynamic of the *readout* layer is trained and thereby updated at each time step.

In the present study, the large randomness of the RC approach to the prediction of a chaotic system, such as the Lorenz system, is described. A statistical analysis, based on the Projection of Proper elements method [10, 11], is thus carried out to validate and evaluate the accuracy of the RC method application. The random-

ness is demonstrated to be related to the random initialisation of the reservoir network components, and highly affected by the chosen configuration parameters. Large variation of the error in the prediction phase is obtained for a broad set of parameters of the reservoir, leading to strong inaccuracy in predicting the time evolution of the Lorenz chaotic trajectories for a significant sample of realisations. The results presented in recent contributions [2, 3] are shown to fall within a narrow region of the scanned parameter series. Nevertheless, the prediction error of such a narrow favorable region is affected by large statistical variation as well, making the AIS prediction of chaotic trajectories frequently not reliable.

The remainder of the paper is organized as follows: the specific RC approach that has been applied on the Lorenz system [1] and the evaluation techniques, including the Projection on Proper elements method [10, 11], are described in Section II; Section III is subdivided in five subsections, illustrating the principal results that are achieved. Different hyper-parameters of the reservoir network and of the model are considered and deeply analyzed, with statistical insight of the probability distribution function of the errors; dedicated analysis on the time evolution of the Lorenz coefficients is carried out; the main conclusions are summarized in Section IV.

II. METHODOLOGY

In this paper we produce the database by solving the Lorenz system given by eq. 1 using a 4th order Runge-Kutta method (RK4). This integration will produce the data set $\{x_i, y_i, z_i\}$, with N the maximum number of time steps. We will use $\Delta t = 0.02$ and $N = 6250$. Such data set will be divided into a training set and a prediction set, with respective lengths $N_{\text{train}} = 5000$ and $N_{\text{pred}} = 1250$, such that $N = N_{\text{train}} + N_{\text{pred}}$. The training set will be used to compute the parameters of the AIS and the prediction set will be used to test the predictive capabilities of the AIS.

A. Reservoir Computing Setup

Here we follow exactly the methodology employed by Pathak et al. in Refs. [2, 3] with the same set of parameters they used to build the RC. The architecture of the AIS is shown in figure 1 and will be briefly explained in the following. The input vector is called $\mathbf{u}(t) \in \mathbb{R}^3$ and contains the three components of the Lorenz system, x , y and z . It is fed into the *reservoir*, represented by a square matrix whose element (i, j) indicates the connection between the neuron i and the neuron j . Such matrix is called $\mathbf{A} \in \mathbb{R}^{D_r \times D_r}$, with D_r the number of neurons. If the element $A_{i,j} = 0$, the neurons i and j are not connected. Between the input and the reservoir, one needs an input layer $\mathbf{W}_{in} \in \mathbb{R}^{3 \times D_r}$, mathematically representing an application from \mathbb{R}^3 to \mathbb{R}^{D_r} . Both the

reservoir matrix and the input layer are randomly initialised. The elements of both \mathbf{W}_{in} and \mathbf{A} are drawn from a uniform distribution function in $[-1, 1]$, with an additional multiplying scaling factor $\gamma_{scal} = 0.1$ applied only to the input layer elements. The elements of the reservoir are re-scaled so that the largest magnitude of the eigenvalues (the so-called spectral radius) is equal to the desired value ρ . In the present study, based on the example of Refs. [2, 3], the *reservoir* matrix \mathbf{A} is given by a sparse Erdős-Rényi network [12, 13], with an average degree of $d = 6$. It is to be noted that, since the degree of the Erdős-Rényi network is fixed to $d = 6$, the rewiring probability $p = d/D_r$ is decreased (increased) when D_r is increased (decreased) and therefore the connectivity matrix of the neural network becomes sparser (less sparse). As it will be presented in the following, the number of reservoir neurons and the spectral radius of the adjacency matrix are widely scanned and the impact of each couple of input parameters on the measured errors is then evaluated. Each neuron of the reservoir is characterised by a state $\mathbf{r}(t)$, which represents the activation of the neuron (-1 : de-activated, $+1$: activated), computed at each time step by a *tanh* activation function:

$$\mathbf{r}(t + \Delta t) = \tanh(\mathbf{A} \cdot \mathbf{r}(t) + \mathbf{W}_{in} \cdot \mathbf{u}(t)) \quad (2)$$

The particular choice of using the activate function of equation 2 is made in order to follow the example of Refs. [2, 3, 5]. The underlying idea of the reservoir computing is to predict the dynamic of the system at the time step $n + 1$, i.e. \mathbf{u}_{n+1} by means of the relation:

$$\mathbf{u}_{n+1} = \mathbf{W}_{out} \cdot \mathbf{r}_n + \mathbf{c}_{out} \quad (3)$$

The weights of the *readout* layer $\mathbf{W}_{out} \in \mathbb{R}^{3 \times n}$ can be subsequently computed by minimizing the difference between the actual $\mathbf{u}(t)$ and the predicted $\mathbf{v}(t)$ Lorenz trajectories for each time step of the training phase. Therefore, in order to train the reservoir computing, one has to minimize \mathbf{W}_{out} and $\mathbf{c} \in \mathbb{R}^3$ in the following quadratic form:

$$\|\mathbf{W}_{out} \cdot \mathbf{r} + \mathbf{c} - \mathbf{v}\|^2 \quad (4)$$

for all the time step of the training phase, where $\|\mathbf{q}\|^2 = \mathbf{q}^T \cdot \mathbf{q}$. Please note that the so-called "ridge regression parameter" $\beta = 0$, as in the case here studied the overfitting was already avoided [2]. Then, this minimization problem reduces to a linear regression, whose solution in the training phase is:

$$\mathbf{W}_{out}^* = (\mathbf{U} \cdot \mathbf{R}^T) \cdot (\mathbf{R} \cdot \mathbf{R}^T)^{-1} \quad (5)$$

where $\mathbf{U} \in \mathbb{R}^{3 \times n}$ is the array containing the actual dynamics of the Lorenz system, $\mathbf{R} \in \mathbb{R}^{3 \times n}$ the array containing the neuron states and \mathbf{W}_{out}^* is the particular solution of the minimization problem. As a result, the *readout* layer \mathbf{W}_{out} is trained and thereby fixed. Hence, the

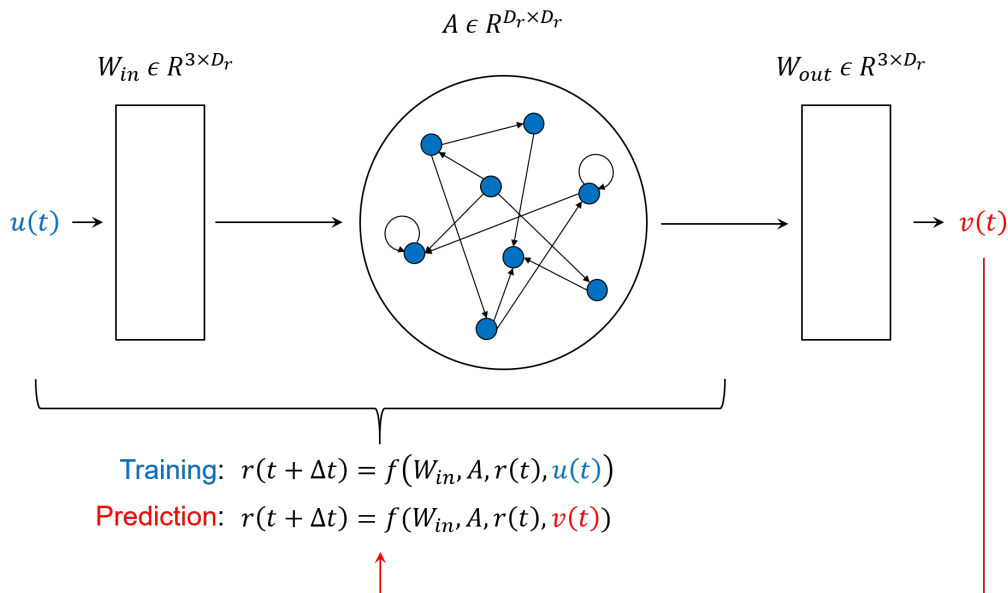


FIG. 1: Schematic representation of the reservoir computing paradigm.

same procedure can be applied in the prediction phase. Indeed, the neuron states are now computed using the predicted vector by:

$$\mathbf{r}(t + \Delta t) = \tanh(\mathbf{A} \cdot \mathbf{r}(t) + \mathbf{W}_{in} \cdot \mathbf{v}(t)) \quad (6)$$

and subsequently applied as:

$$\mathbf{v}_{n+1} = \mathbf{W}_{out} \cdot \mathbf{v}_n \quad (7)$$

for the entire prediction phase. The vector $\mathbf{v}_{n+1} = [\tilde{x}, \tilde{y}, \tilde{z}]_{n+1}$ contains the components of the Lorenz dynamics predicted by the RS approach at the time step $n + 1$.

It is to be noted that the assumption of symmetry in computing the first two components $x \rightarrow -x$ and $y \rightarrow -y$ of the Lorenz equations [2, 5] in the predicted vector \mathbf{v} is retained, in order to be consistent with the assumption made in Refs. [2, 3, 5]. As the considered chaotic system could be not predetermined likewise the well-known Lorenz model, the same analysis has been carried out relaxing the symmetry hypothesis. Nevertheless, very similar results are obtained when such an assumption is relaxed.

Table I summarizes the principal parameters of the analyzed RC configurations.

B. Error Quantification through the PoPe Method

The AIS predictive capabilities were evaluated in Refs. [2, 3] based on the ability to predict the *climate*,

TABLE I: Reservoir parameters that has been used for the standard simulations, if not otherwise clearly noted.

As explained in the main body of the Letter, the parameters are: β the ridge regression parameter, γ_{scal} the scaling factor applied to the input layer \mathbf{W}_{in} , D_r the reservoir number of neurons, ρ the spectral radius of the reservoir network, d the average degree of the Erdős-Rényi network, Δ_t the time step of the considered Lorenz dynamics, n_{train} and n_{pred} the number of time step in the training and prediction phase respectively, and δ the period of the moving time window for the error calculation. Very similar parameters have been used also in Ref. [2].

Parameter	Value
β	0
γ_{scal}	0.1
D_r	[50, 610]
ρ	[0.5, 2.5]
d	6
Δ_t	0.02
n_{train}	5000
n_{pred}	1250
δ	1.25

i.e. the ergodic properties of the chaotic system quantified by the Lyapunov exponents. In the present Letter, we employed a different criterion, based on the Projection on Proper elements (PoPe) using the Euclidean distance as the measure to quantify the error of the system to reproduce the chaotic behaviour. The PoPe method is described in detail in Refs. [10, 11] and here we provide only a brief explanation for our purposes. Let us note that the Lorenz system can be rewritten as follows

$$\begin{cases} \dot{x} = a(y - x) + \alpha_x & (8a) \\ xz + y + \dot{y} = bx + \alpha_y & (8b) \\ -xy + \dot{z} = -cz + \alpha_z & (8c) \end{cases}$$

It can be observed that this system takes the form of a linear system

$$\mathcal{Y} = \boldsymbol{\alpha} + \mathbf{m} \odot \mathcal{X} \quad (9)$$

Note that whereas \mathcal{X} is straightforwardly given at any point of the dataset, the vector \mathcal{Y} requires the computation of the time derivatives, which can be done with arbitrarily high precision. Note also that another way to measure the prediction error can be used, where the distance between the exact and the predicted trajectory are computed. However, for chaotic time series this is not a useful quantity, since any small error get amplified and therefore. This means that even though the systems are physically close to each other, their time series can be very disparate. For this reason, we better quantify the prediction error through Eq. 10. Moreover, the prediction error is computed based on the coefficients $a^*, b^*, c^*, \alpha_x^*, \alpha_y^*, \alpha_z^*$ via a linear regression using $3n_{\text{pred}}$ data points. Therefore, the prediction error may depend on the length of the prediction phase n_{pred} .

In addition to ϵ_{pred} , to quantify to which extent the prediction error is reliable we calculate the mean squared error for each coordinate as

$$MSE_{\chi} = \frac{1}{N_{\text{pred}}^{\text{max}}} \sum_{j=1}^{N_{\text{pred}}^{\text{max}}} (F_{\chi}(\tilde{x}_j, \tilde{y}_j, \tilde{z}_j; \mathcal{P}_{\chi}) - \dot{\chi}_j)^2 \quad (11)$$

with $\chi \in \{\tilde{x}, \tilde{y}, \tilde{z}\}$ and $\mathcal{P}_{\tilde{x}} = a^*$, $\mathcal{P}_{\tilde{y}} = b^*$ and $\mathcal{P}_{\tilde{z}} = c^*$. Since the MSE depends on the coordinate to be analysed, we determine the $RMSE_{\text{max}} \equiv \max_{\chi} (RMSE_{\chi})$, where $RMSE_{\chi} = \sqrt{MSE_{\chi}}$, since this criterion is more penalizing.

In this paper, we will quantify the performance of the RC approach to predict chaotic trajectories through a scan on the number of neurons D_r and the spectral radius of the Erdős-Rényi network. In addition, we will explore the impact of the length of the prediction phase on the prediction error 10. As already stated, the RC approach is based on the fact that all the parameters of the system are initialised randomly, except those of the output layer. This implies that the training phase is reduced to a simple linear regression. But this also

with $\mathbf{m} = (a, b, c)$ and \odot an element-wise multiplication operator. Let us now assume that we have a set of data $\{x_i, y_i, z_i\}_{1 \leq i \leq n_{\text{train}}}$ produced by an AIS during the prediction phase and let us assume that we want to determine to what extent this set of data has been generated by the Lorenz system given by equation 1. To answer this question we can determine the parameters \mathbf{m}^* and $\boldsymbol{\alpha}^*$ which better fit the data and compare them to the ones that were used for the integration of the Lorenz system, namely $(a, b, c, 0, 0, 0)$. Such comparison provides the error ϵ_{pred} between the numerical integration of 1 (what we call the *exact* solution) and the prediction made by the AIS. The error is expressed as

$$\epsilon_{\text{pred}} = \sqrt{(a - a^*)^2 + (b - b^*)^2 + (c - c^*)^2 + \alpha_x^{*2} + \alpha_y^{*2} + \alpha_z^{*2}} \quad (10)$$

implies that the results may depend on the random initialisation of the parameters. To overcome this difficulty, for each point in our scan (D_r, ρ) , we perform $N = 500$ realisations. Each of them will be different, since the initialisation of the network and of the input layer is random. For each realisation s we calculate $\epsilon_{\text{pred}}^{(s)}$ and $RMSE_{\text{max}}^{(s)}$ and we use the two ensemble averaged quantities, $\langle RMSE_{\text{max}} \rangle_{\text{rls}} = \frac{1}{N} \sum_s RMSE_{\text{max}}^{(s)}$ and $\langle \epsilon_{\text{pred}} \rangle_{\text{rls}} = \frac{1}{N} \sum_s \epsilon_{\text{pred}}^{(s)}$.

The prediction error and the $RMSE$ can be calculated in two different ways: (1) for time windows whose left endpoint is set to 0 and the right endpoint is upper-bounded by $t_{\text{pred}} = 25$ and increasing for each time window as $\kappa\delta$, with $\delta = 1.25$ and $\kappa \in [1, 2, \dots, n]$ denoting the number of the time window; (2) for moving time windows of the same length and whose endpoints are increasing as $[\kappa\delta, (\kappa + 1)\delta]$, with $\delta = 1.25$ and $\kappa \in [0, 1, 2, \dots, n]$. In other words, in the first way the error is computed over time windows whose lengths are increasing, considering therefore the dynamics from $t_{\text{pred}} = 0$ up to $\kappa\delta$; and in the second way, the error and the RMSE are calculated over moving time windows of fixed length $\delta = 1.25$. In the following, we use the first method to compute the errors. We call this method increasing-time-window procedure. In this way the dynamics of the entire considered prediction phase is taken into account in calculating the deviation from the actual Lorenz trajectories. Nonetheless, it could be useful to compare these results with the moving average error, i.e. the second procedure described here above, as it is done for instance in section III C. The choice of the time window length of $\delta = 1.25$ yields a sufficient number of points to calculate the linear regression and the subsequent predicted coefficients $(a^*, b^*, c^*, \alpha_x^*, \alpha_y^*, \alpha_z^*)$ in each time window of the moving error procedure. However, if not otherwise noted, the standard procedure for computing the errors and the RMSE is the increasing-time-window procedure.

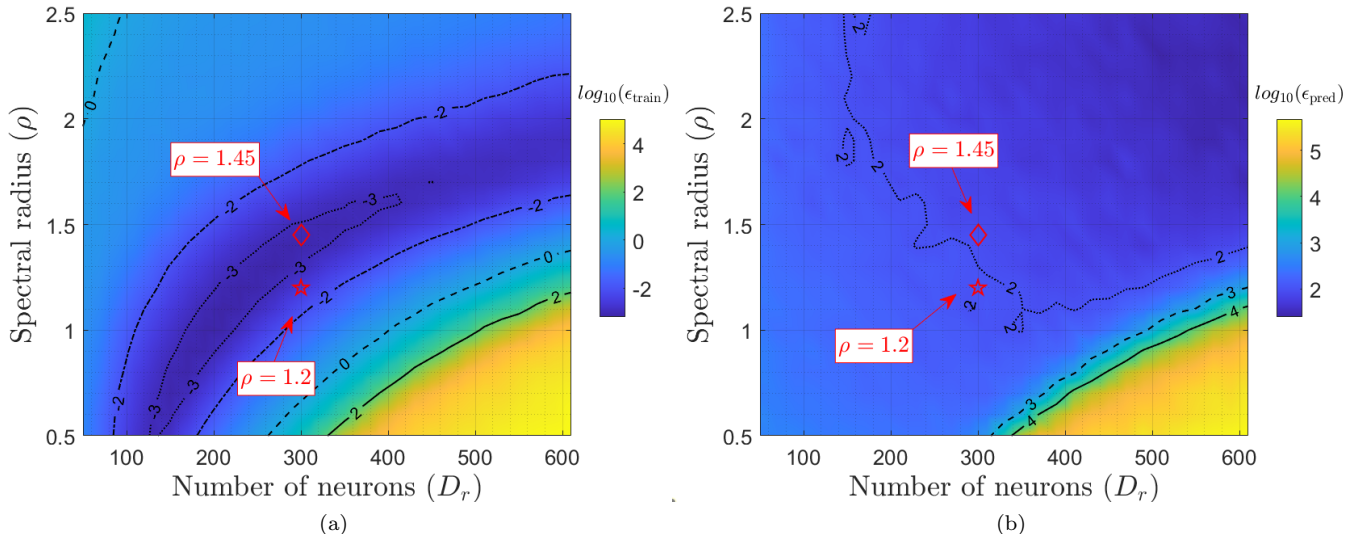


FIG. 2: A scan of the error 10, in logarithmic scale, over the input parameters D_r and ρ of the reservoir network is displayed for the training and the prediction phase, in panel (a) and (b) respectively. The errors are averaged over the whole set of realisations ($N = 500$) for each couple (D_r, ρ) . Highlighted with red markers are the configuration employed in Ref. [2].

Finally, it is also instructive to quantify the training error ϵ_{train} , which is computed using the same Euclidean distance as in equation 10, but applied only to the training phase.

III. RESULTS

The training and prediction errors averaged over all the realisations are plotted in figures 2(a) and (b), respectively, fixing the length of the prediction phase to $t_{\text{pred}} = 25$, i.e. $n_{\text{pred}} = 1250$. The isocontours of the averaged training and prediction errors are represented in logarithmic scale as a function of the number of neurons D_r and the spectral radius ρ of the reservoir network. The error in the prediction phase is calculated for the entire prediction time, i.e. $t_{\text{pred}} = [0, 25]$. It is observed that the training error is minimum in a rather narrow region in the (D_r, ρ) plane. Moreover, mild variations of (D_r, ρ) may lead to an abrupt increase of the training error. This means that there is a strong restriction in the allowed values of D_r and ρ . It is particularly important to realise that increasing the number of neurons does not necessarily reduce the averaged training error. Moreover, we can observe that the averaged prediction error is significant, increased by several orders of magnitude with respect to the training error. The values selected in [2] were $D_r = 300$ and $\rho \in \{1.2, 1.45\}$, which fall into the beneficial narrow region where the training error is minimal, as the markers in figure 2(a) show. Yet, it is observed that the averaged prediction error is far from being negligible, considering the entire prediction

phase $t_{\text{pred}} = 25$. Within the set of scanned parameters in figure 2, a region where $\langle \epsilon_{\text{pred}} \rangle_{\text{rls}}$ is minimized is noted for $D_r > 400$ and $\rho > 1.5$. In the remainder of the paper, such a region, and the configuration included therein, will be called *favorable*. Indeed, the region where $D_r > 300$ and $\rho < 1.2$ presents the largest measured averaged errors of the analyzed range of parameters in the prediction phase. For this reason, it will be termed as the *unfavorable* region of the (D_r, ρ) plane.

A. Large Statistical Variation of the Errors due to Random Initialisation

It is also observed that the averaged errors in both training and prediction phases for each couple (D_r, ρ) may be accompanied by a large variation within the set of performed realisations. In figure 3, the standard deviation σ of the averaged errors within the set of $N = 500$ realisations is plotted as a function of the number of neurons D_r and the spectral radius ρ for the training and the prediction phases in (a) and (b), respectively. The set of realisations is the same displayed in figure 2, and the errors shown in panel (b) for the prediction phase are calculated for $t_{\text{pred}} = [0, 25]$, consistently with figure 2. The large dispersion that can be appreciated by measuring σ demonstrates the strong impact of the randomness on the prediction of Lorenz chaotic trajectories by the RC technique. The plot in figure 3(a) provides additional evidence that the possible efficient configurations of this AIS based on the RC approach for the prediction of chaotic trajectories are limited to a narrow region in

the (D_r, ρ) plane. Furthermore, similarly to what has been observed in figure 2, the difference of the standard deviation for the set of realisations between the training phase and the prediction phase is significant, especially in the *favorable* region of the scan. Indeed, this proves the more frequent occurrence of large error events in the prediction phase, which are then responsible also for the increase of the averaged prediction error within the set of the realisations with respect to the training phase.

Insightful information on the randomness of the RC prediction can be found by further analysing the two specific study-cases described in Ref. [2]. From the statistically-relevant averaged results illustrated in figure 2, one can infer that the case with $(D_r, \rho) = (300, 1.45)$ performs better than the case with $(D_r, \rho) = (300, 1.2)$ (respectively, red diamond and red star in figure 2), as the $\langle \epsilon_{\text{pred}} \rangle_{\text{rls}}$ is minor for the former than for the latter case. This result might not be in full agreement with what is reported in Ref. [2], where the case with $(D_r, \rho) = (300, 1.45)$ is shown to be less performing to predict chaotic trajectories, with respect to the case with $(D_r, \rho) = (300, 1.2)$. This might be due to the random initialization of the input layer and the reservoir array. Indeed, for one single realization, the case with $(D_r, \rho) = (300, 1.2)$ can perform better than that with $(D_r, \rho) = (300, 1.45)$, consistently with Ref. [2]. This is illustrated in figure 4, where the time traces of x , y and z are plotted for $D_r = 300$ and the two values $\rho = 1.2$ (left panel) and $\rho = 1.45$ (right panel). In each panel, the realisation with minimum error is plotted by a red curve. Another randomly chosen realization is plotted by the blue curve. As a reference, the exact solution is given by the dashed black curve. It is observed that depending on the realization, the case $\rho = 1.2$ can perform better or worse than the case $\rho = 1.45$.

B. Statistical Analysis on the Error Distribution

Given the large statistical variation exhibited by the measured errors, we analyse the relevance of using the mean value as an indicator of the error for each single (D_r, ρ) configuration within the set of realisations. The histograms of $\log_{10}(\epsilon_{\text{pred}})$ for four couples (D_r, ρ) configurations are shown in figure 5. The same analysis on the error in the training phase $\log_{10}(\epsilon_{\text{train}})$ revealed analogous results. These four different cases are chosen to represent: (a) a *favorable* case, (b) and (c) the same cases studied by Pathak et al. in Ref. [2] and (d) a case in the *unfavorable* region of the (D_r, ρ) plane. In this particular analysis, the number of realisations has been increased up to $N = 5000$ to improve the statistical relevance of the data set, and the histograms are captured in $n_{\text{bins}} = 100$ bins evenly spaced. As can be seen, the histograms are shifted to large error values going from panel (a) to panel (d). In the four panels, the Gaussian probability density function (PDF), whose mean and standard deviation are respectively equal to the statistical mean

and standard deviation of the corresponding set of realisations, is over-plotted with black dashed lines. In this way, it is straightforward to compare the histograms and the Gaussian PDFs. Whereas for panels (b) and (c) the distribution of the error over the set of realisations follows a Gaussian, for panels (a) and (d) the histograms exhibit a departure from the normal PDF. In particular for the configuration $(D_r, \rho) = (550, 0.9)$, an inset with the rightmost tail of the distribution function is displayed in a log-log plot. In this way, it is possible to appreciate the deviation for the large-error events of such configuration from the tail of the Gaussian distribution. This deviation is present in all the analyzed configurations of the *unfavorable* region of the (D_r, ρ) plane. Therefore, it is demonstrated the accuracy of using the statistical mean, i.e. the first moment of the distribution function, to quantify the error in both training and prediction phases for a significant range of analyzed configurations. Yet, the *unfavorable* region of the (D_r, ρ) plane presents a non-negligible deviation from the Gaussian distribution, especially concerning the large error events.

Additionally, it could be observed that the slight deviation of the histograms from the normal distribution function, especially in panel (d), can be explained by studying the third and fourth standardized moments of the PDF, i.e. the skewness μ_3 and the kurtosis μ_4 respectively. The skewness measures the loss of asymmetry of a distribution function. For a symmetric PDF the skewness is null ($\mu_3 = 0$), hence a positive (negative) value indicates that the data-set is skewed to the right (left) with respect to the principal mode - the mean value for a unimodal Gaussian PDF. On the other hand, the kurtosis property measures the flatness of the PDF. Generally, the kurtosis is compared to the kurtosis of a Gaussian distribution function, which is equal to 3 ($\mu_4 = 3$). Therefore, it is commonly used the excess kurtosis $\tilde{\mu}_4$, which is the kurtosis re-scaled to 3 ($\tilde{\mu}_4 = \mu_4 - 3$). A large excess kurtosis thus indicates that the distribution has strongly populated tails. Therefore, by inspecting the loss of asymmetry (skewness) and strength of the tails (excess kurtosis) together, it is possible to evaluate the behaviour of the measured PDFs. The measured distribution function in figure 5(a) and (d) reveal a positive skewness, denoting a major broadening towards large error values, as can be also inferred from the plots. Whereas for the configuration $(D_r, \rho) = (470, 2.2)$ the skewness is mildly above zero, the RC with $(D_r, \rho) = (550, 0.9)$ shows a four-time larger value of the skewness, which evidences the more frequent occurring of large error events. For this latter configuration the re-scaled fourth moment, the excess kurtosis, is positive and large indicating that the distribution of the data-set is strongly peaked around the mean value. In conclusion, the statistical properties of the cases in panels (a), (b) and (c) indicate that the distribution functions could be well approximated with a Gaussian around the corresponding mean values. On the other hand, for the unfavorable case in panel (d), the statistical mean value is strongly affected by a more

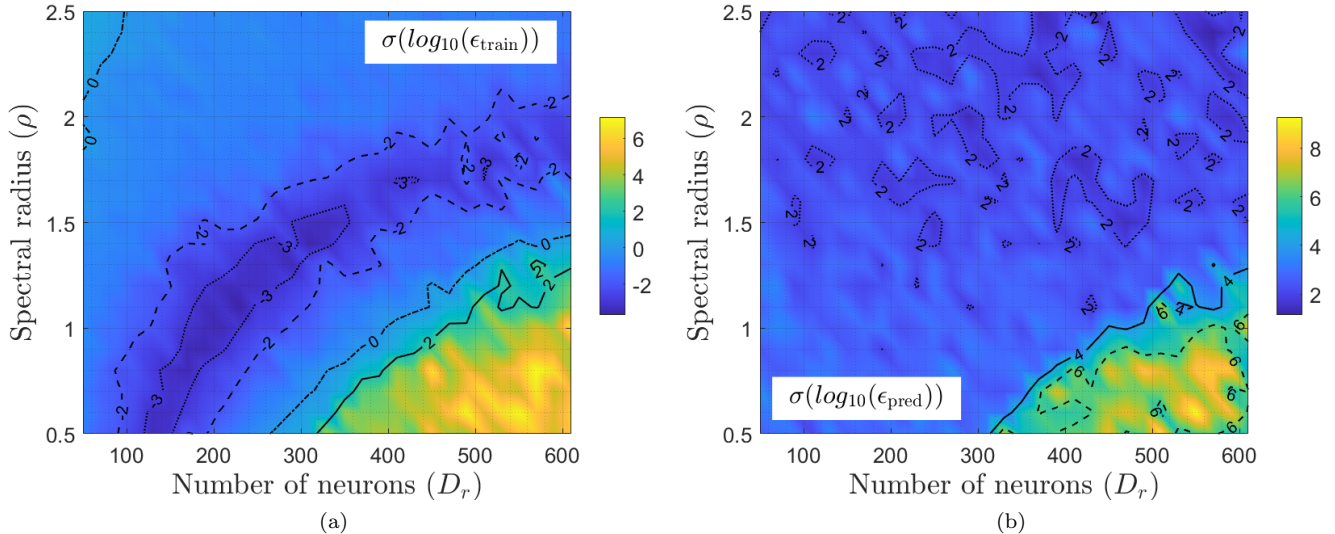


FIG. 3: The standard deviation σ of the logarithm in base 10 of the errors, for both training (a) and prediction (b) phases, within the set of $N = 500$ realisations is displayed for the same scans reported in figure 2. The large variation within the whole set of realisations can be thus appreciated.

frequent occurring of large-error events.

C. Dependence of the Error on the Prediction Phase Length

To shed some light on the validity of the RC to predict chaotic trajectories, we additionally explore the dependence of the prediction error on the maximum length of the prediction phase. As illustrated in Ref. [2], the AIS based on the RC approach correctly predicts the short-term trajectories, while significantly deviating from the actual Lorenz trajectories in the long-term phase. The considered length of the prediction phase has thereby a strong impact on the computed error. Therefore, we analyse the dependence of the averaged prediction error and $\max_{\chi}(RMSE_{\chi})$ on the length of the prediction phase in the two different procedures that have been described at the end of section II B. The results are illustrated in figure 6. Hence, in panels (a)-(c) the prediction error and the $RMSE$ are calculated for time windows whose period is $[0, \kappa\delta]$, with $\delta = 1.25$ and $\kappa = [1, 2, \dots, n]$, up to $t_{\text{pred}} = 25$. Indeed, panels (d)-(f) represent the prediction error and the $RMSE$ calculated in the second fashion, for which the period of the time windows is $[\kappa\delta, (\kappa + 1)\delta]$, with $\delta = 1.25$ and $\kappa = [0, 1, 2, \dots, n]$. The two procedures are labelled in the figure as increasing-time-window average error and moving average error, respectively.

As it has already been noted, even for the favorable cases in panel 6(a) in previous sections, both $\langle \log_{10}(\epsilon_{\text{pred}}) \rangle_{\text{rls}}$ and $\langle \log_{10}(RMSE_{\text{max}}) \rangle_{\text{rls}}$ indicators are very large compared to the error in the corresponding

training phase. It is also observed that there is a strong dependence on the length of the prediction phase in the short-term prediction. Focusing on the increasing-time-window average procedure, after the prompt increase in the short-term prediction, the error remains constant (after an elbow) in the long-term prediction, consistently with Ref. [2]. Such a behaviour is actually present for the *favorable* configurations also when the error is calculated with the moving average procedure, as panels (d) and (e) show.

Furthermore, smoother curves in the time evolution of the calculated error appear when the increasing-time-window average procedure is employed. This is to be understood as, in this latter procedure, the calculation has a kind of 'memory' from previous time windows, since the analyzed time period increases by including also the dynamics of the previous time windows. On the other hand, there is no such 'memory effect' in the moving average procedure, as the solution coefficients are calculated for each time window independently from the previous ones.

Another striking observation comes from the value of the error at the end of the first time period of the prediction phase ($t_{\text{pred}} \in [0, 1.25]$). Indeed, the average prediction error $\langle \epsilon_{\text{pred}} \rangle_{\text{rls}}$ already presents value much larger than the error evaluated for training phase for the same configuration. The difference between these two values can also be inferred from the plots in figure 2. Especially for the *favorable* configurations, the difference could be also more than 4 orders of magnitude. Therefore, the RC approach could show a strong disparity from the expected dynamics also for $t_{\text{pred}} < 2.5$, i.e. for only 3 ~ 4 oscillations of the Lorenz system. This could essentially be due to two reasons: either the reservoir layers are failed

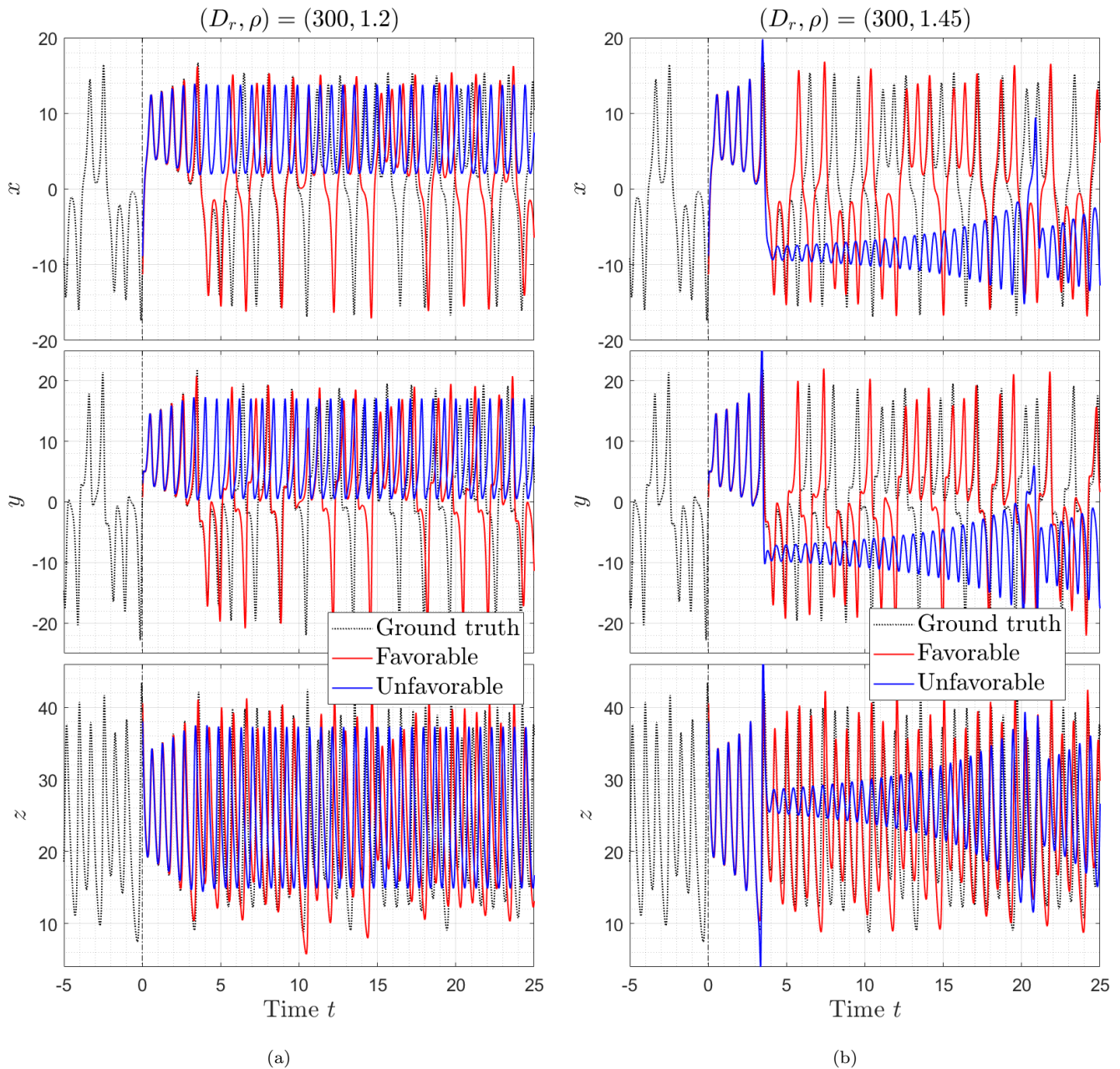


FIG. 4: The dynamics of the three components of the Lorenz system, predicted by the RC, is shown for the two configurations studied in Ref. [2], i.e. $(D_r, \rho) = (300, 1.2)$ (a) and $(D_r, \rho) = (300, 1.45)$ (b). The blue dashed curves are the actual chaotic trajectories obtained through numerical integration of the Lorenz equations with RK4 method. Red and green curves show respectively the best and a non-favorable solution obtained through RC technique over the whole set of $N = 500$ realisations.

to be trained and the error is thereby propagated in the prediction phase inevitably, or the RC technique predicts strongly different dynamics in the short-term phase. The former condition, for which the training phase already produces a large error and thus the reservoir layers are not well-trained, is less frequent, as the lower mean values of the error in figure 2(a) and the standard devi-

ations in figure 3(a) illustrate. Nevertheless, if a large error event occur in the training phase, this inevitably produces a large error event also in the prediction phase, since the RC is ill-trained and so unable to recover the correct Lorenz dynamics. The latter condition, for which the RC network is well-trained but fails in predicting the short-term dynamics, is indeed the most frequent. As a

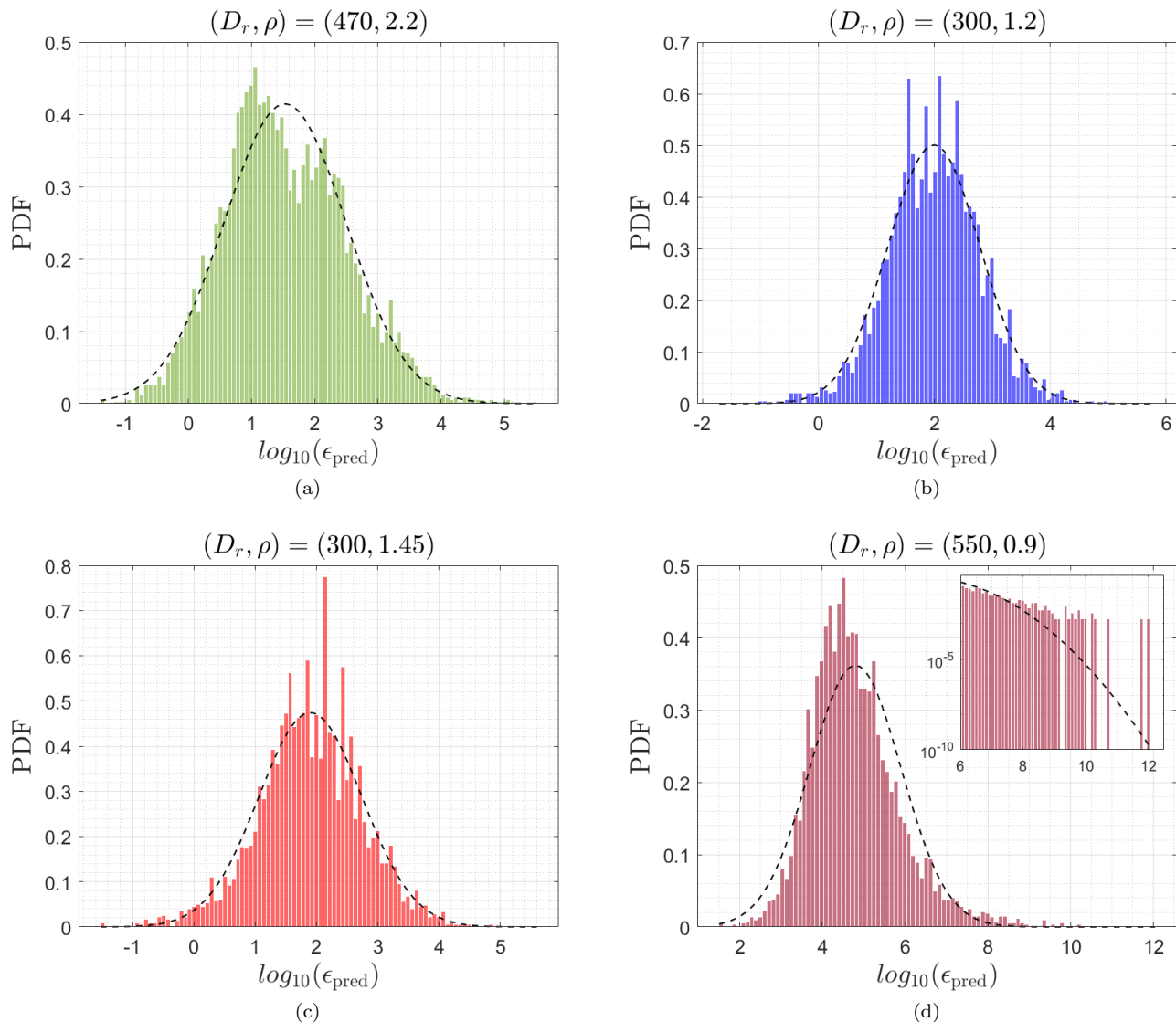


FIG. 5: The error in logarithmic scale in the prediction phase, calculated at $t_{\text{pred}} = 25$, of an incremented set of $N = 5000$ realisations is shown in histogram plots for four different RC configurations. The distribution is binned in $n_{\text{bins}} = 100$ samples. The black dashed curves represent the unimodal normal PDF, whose mean value and standard deviation are the mean value and the standard deviation of the error distribution functions for the corresponding configuration.

result, the average error in the first time window of the prediction phase is much higher than the one measured in the training phase.

D. Dependence of the Error on the Train Phase Length

It is now considered the effect of the length of the training phase on the error in predicting the Lorenz trajectories by means of the RC technique. In figure 7, the dependence of both $\langle \epsilon_{\text{train}} \rangle_{\text{rls}}$ and $\langle \epsilon_{\text{pred}} \rangle_{\text{rls}}$ on the length of the training phase is displayed for various chosen reser-

voir configurations. The plots illustrate the result for $n_{\text{train}} > 1000$, as for smaller number of time steps the RC definitely fails in being trained and subsequently in predicting the chaotic dynamic of the system. The parameters of the various configurations are the same analyzed in panels (a) and (b) (and also (d) and (e)) of figure 6. The error in the prediction phase is considered for the entire prediction phase $t_{\text{pred}} = [0, 25]$. A striking observation about the training phase for the configurations with $(D_r, \rho) = (430, 2.3)$ and $(D_r, \rho) = (470, 2.2)$ is the non-monotonic behaviour of the function. Indeed, for a narrow range of the training phase length, the $\langle \epsilon_{\text{train}} \rangle_{\text{rls}}$ curves presents a minimum. Such a behaviour has been

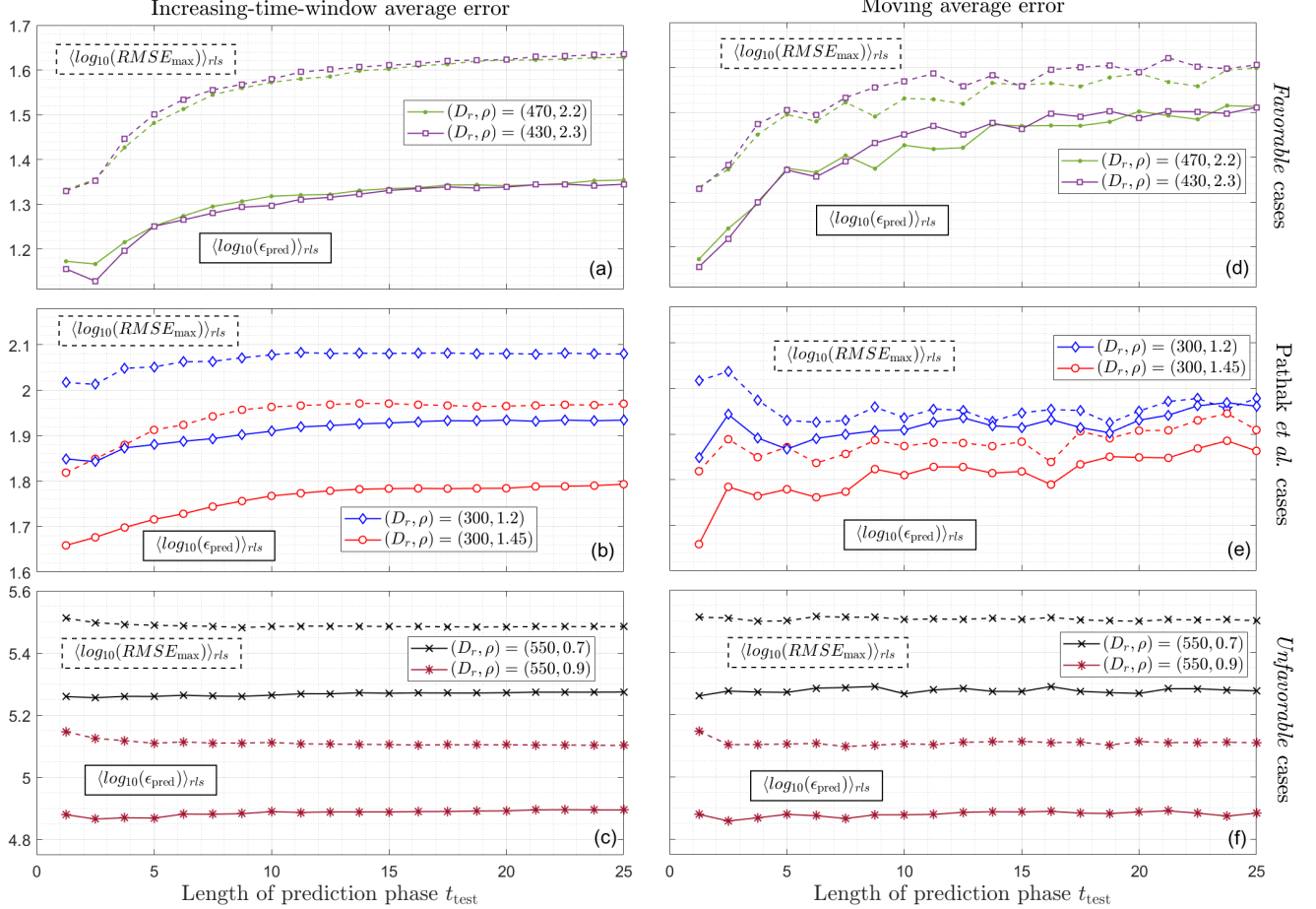


FIG. 6: The error in the prediction phase is displayed as a function of the length of the prediction phase for different configurations. The error and RMSE are calculated at increasing width of the time windows in panels (a)-(c), whereas with moving time window of fixed period $\delta = 1.25$ in panels (d)-(f). The configurations reported are picked from the whole scanned cases, with the purpose of representing: (a) and (d) favorable cases, (b) and (e) the same cases reported in Ref. [2] and eventually (c) and (f) cases from the unfavorable region of the (D_r, ρ) plane explored in figure 2.

found also in other configurations within the *favorable* region of the (D_r, ρ) plane. Instead, for the configuration setups with $(D_r, \rho) = (300, 1.2)$ and $(D_r, \rho) = (300, 1.45)$, the same analyzed by Pathak et al. in [2], the error in the training phase is basically decreasing with the increasing number of considered time steps for training the system until a plateau is reached. This plateau could be expected due to the quasi-periodicity of the chaotic oscillations of the Lorenz system. Regarding the prediction phase, the behaviours of all the detailed configurations resemble. After a sharp decrease for $n_{\text{train}} > 1000$, the curves mildly continue to decrease until $n_{\text{train}} = 4000 \sim 5000$, where they become averagely constant. Therefore, the increase of the number of time steps in the training phase beyond $n_{\text{train}} = 10000$ leads to enhanced elapse time and complexity of the system, without improving the prediction of the chaotic trajec-

tories significantly. Furthermore, it is to be noted the jagged behaviour of $\langle \epsilon_{\text{pred}} \rangle_{\text{rls}}$ in function of the number of time steps n_{train} . Consecutive points of this particular scan could lead to very different results. Thus, increasing n_{train} does not automatically lead to an improvement of the results, but it could be indeed detrimental in average.

E. Studies on the Time Evolution of the Predicted Lorenz Coefficients

Additional analyses have been carried out on the evolution in time of the coefficients $(\tilde{a}, \tilde{b}, \tilde{c}, \tilde{\alpha}_x, \tilde{\alpha}_y, \tilde{\alpha}_z)$ which better fit the prediction obtained by means of the RC technique. In the Lorenz system, such coefficients are constant throughout the whole time trajectory. This assumption, together with the constraint of having

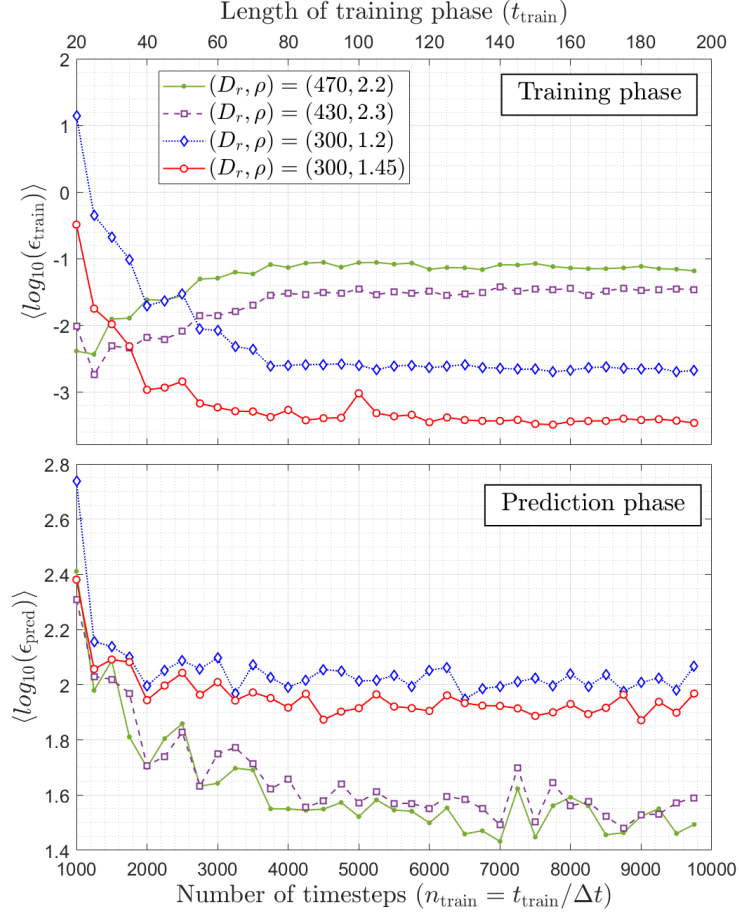


FIG. 7: The errors in the training (a) and in the prediction phase (b) are shown as a function of the length of the training phase for four different input configurations of the reservoir network. The configurations are the same analyzed also in figures 5 and 6. The abscissas is expressed both in length of the training phase in normalized time t_{train} and in number of timesteps n_{train} in the training phase.

$(\tilde{\alpha}_x, \tilde{\alpha}_y, \tilde{\alpha}_z) = (0, 0, 0)$, is crucial for the validity of the Lorenz system. Therefore, in order to ensure the reliability of the predicted dynamics of the chaotic system, the fitted coefficients have been plotted for two different RC configurations, which minimizes the prediction error at the end of the prediction phase $\epsilon_{\text{pred}}(t_{\text{pred}} = [0, 25])$, in figure 8. These two configurations are the same analyzed by Pathak et al. in [2], i.e. $(D_r, \rho) = (300, 1.2)$ and $(D_r, \rho) = (300, 1.45)$. As it has already been explained, $(\tilde{a}, \tilde{b}, \tilde{c}, \tilde{\alpha}_x, \tilde{\alpha}_y, \tilde{\alpha}_z)$ are the coefficients which better fit the Lorenz equations for the RC predicted dynamics in the prediction phase. In this particular analysis, the coefficients are calculated for consecutive moving time windows of the prediction phase with a period of $\delta = 1.25$. The same procedure has already been described in section III C when the calculation of moving error has been applied to produce the figures 6(d)-(f). We repeat that this choice of $\delta = 1.25$ enables to have sufficient elements in each time window for the calcu-

lation of such predicted coefficients by linear regression techniques and to grasp, thereby, their time dependence in the prediction phase. Thus, in the first two columns of figure 8, the coefficients of the solution are plotted against the time of the prediction phase t_{pred} , while in the rightmost column the actual Lorenz dynamics are compared to each component of the AIS predicted systems. However, it is observed that in this optimized case the setup with $(D_r, \rho) = (300, 1.45)$ performs better than $(D_r, \rho) = (300, 1.2)$, consistently with what is displayed in figures 6(b) and 6(b) and (e). Indeed, the three predicted coefficients for $(D_r, \rho) = (300, 1.45)$ oscillates around the actual initial Lorenz coefficients (a, b, c) (highlighted in black horizontal dashed lines in the panels of the first column) throughout the whole prediction phase. The deviations from the exact coefficients of the studied Lorenz system appear almost negligible ($\pm 5\%$). Regarding indeed the case with $(D_r, \rho) = (300, 1.2)$, a significant deviation is noted in the time window around $t_{\text{pred}} = 11$. Nevertheless, this deviation does not impair

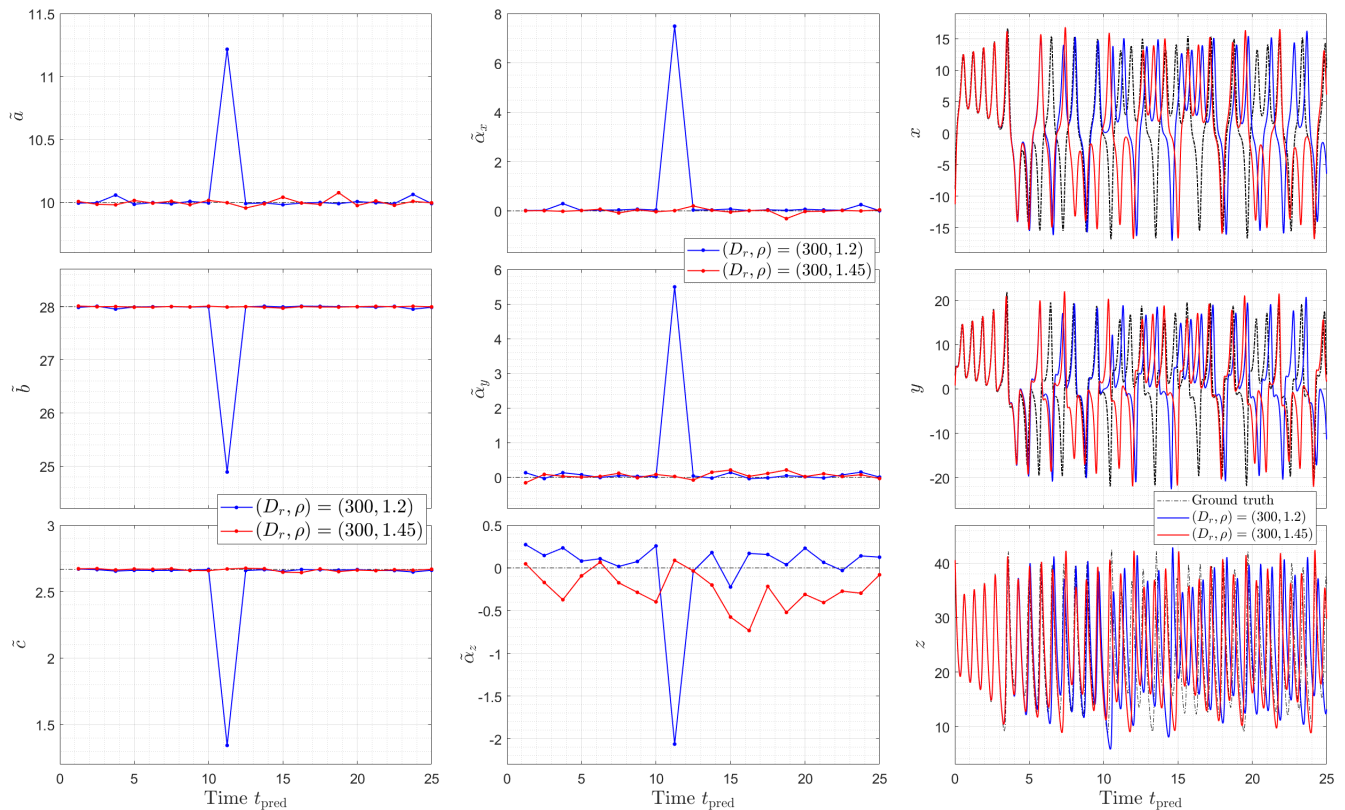


FIG. 8: The coefficients (\tilde{a} , \tilde{b} , \tilde{c} , $\tilde{\alpha}_x$, $\tilde{\alpha}_y$, $\tilde{\alpha}_z$) corresponding to the best solution of the RC application for the configurations also explored in Ref. [2] are shown in the first two columns. The horizontal dashed lines represent the values of the relative coefficients in the actual Lorenz system. In the third column, the predicted dynamics of these two configurations are compared to the actual Lorenz dynamics (labeled 'Ground truth').

the whole prediction phase, as the actual coefficients are promptly recovered after the deviation occurring. If the third column of figure 8 is inspected for the configuration $(D_r, \rho) = (300, 1.2)$ (blue curves), it is possible to see that around $t_{\text{pred}} = 11$ there is a pattern loss, which determines the high spike in the calculation of the predicted coefficients. Yet, such an instantaneous deviation from the exact Lorenz trajectory does not prejudice the overall dynamical properties of the predicted system.

However, as it has already been noted, the solution plotted in figure 8 are the predictions that minimizes $\epsilon_{\text{pred}}(t_{\text{pred}} = 25)$ within a statistically relevant set of $N = 5000$ realisations for each RC configuration. Therefore, the reader must be cautious on evaluating it, since in the same sample of realisations cases with large measured errors were frequently observed, as the average prediction error in figure 2 and the PDF of the prediction error in figure 5 demonstrate. The optimized cases reported in this section, indeed, are located in the tail of the corresponding PDF, and therefore the probability of their occurrence is quite low.

A more detailed analysis on the α coefficients is per-

formed and the results are illustrated in figure 9. Here, the PDF of the α coefficients ($\tilde{\alpha}_x$, $\tilde{\alpha}_y$, $\tilde{\alpha}_z$) for the configuration with $(D_r, \rho) = (300, 1.45)$ is plotted for three different time windows in the prediction phase, i.e. $t_{\text{pred}} = ([0, 1.25], [11, 12.5], [23.5, 25])$. The PDFs are binned in $n_{\text{bins}} = 500$. The same analysis has been carried out also for other configurations in the favorable region of the (D_r, ρ) plane, yielding similar results. What can be inferred here is that the distribution functions of the $\tilde{\alpha}$ coefficients are centered around zero, strongly broadening with increasing time in the prediction phase. Measuring the width of the PDFs, one can notice that it is significantly enhanced going from $t_{\text{pred}} = 1.25$ to $t_{\text{pred}} = 12.5$ for all the three coefficients, whereas no such a difference is measured from $t_{\text{pred}} = 12.5$ to $t_{\text{pred}} = 25$. To corroborate this result, the standard deviation σ of the $\tilde{\alpha}$ coefficients within the set of $N = 5000$ realisations is plotted in logarithmic scale against t_{pred} . The green vertical dashed lines represent the upper boundary of the analyzed time windows. It is observed that already after the first time window, σ increases of more than two orders of magnitude. Then, it reaches a quasi-stationary phase

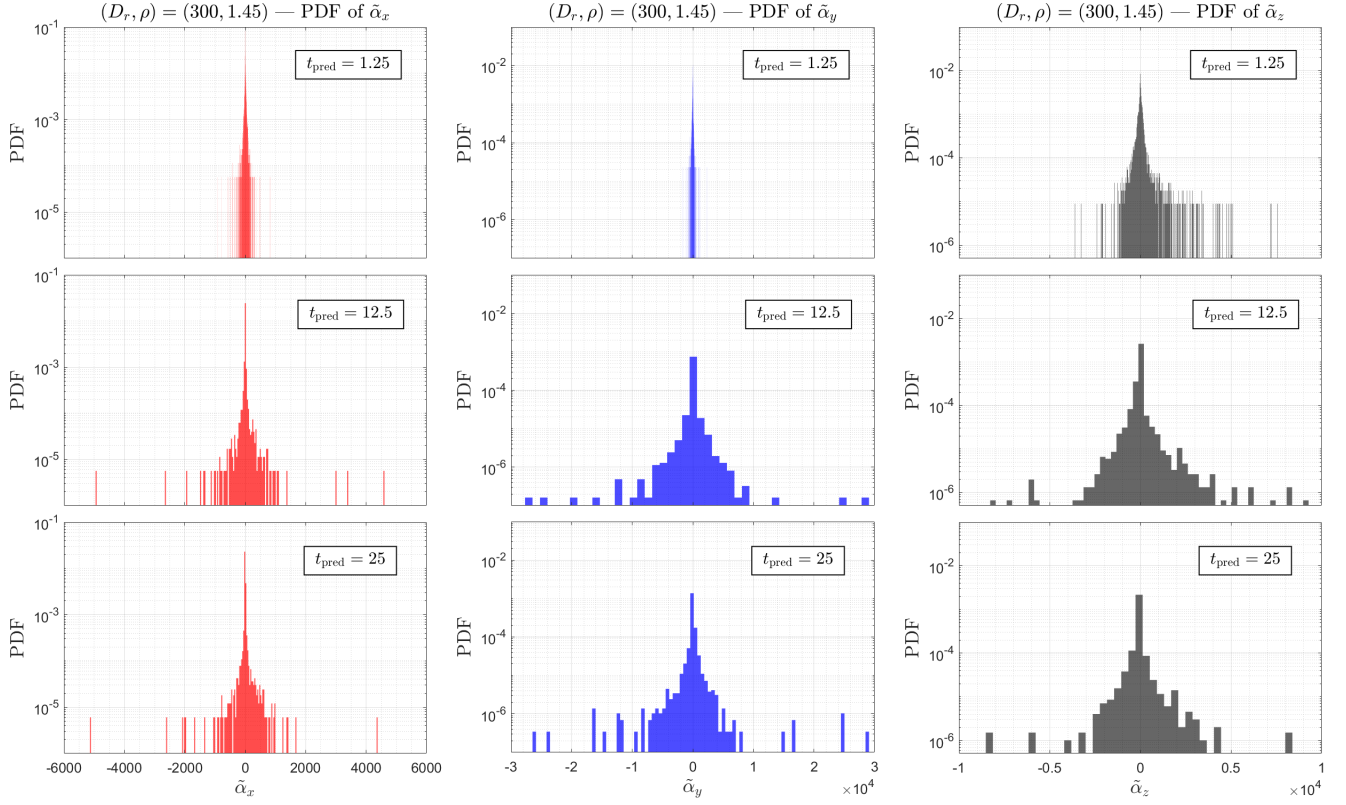


FIG. 9: The probability distribution function of the coefficients ($\tilde{\alpha}_x, \tilde{\alpha}_y, \tilde{\alpha}_z$) for the RC configuration with $(D_r, \rho) = (300, 1.45)$ is shown in histograms for three different time windows of an incremented set of $N = 5000$ realisations. The distribution is binned in $n_{\text{bins}} = 500$ samples. The standard deviation of the PDFs is shown in figure 10 for the entire prediction phase.

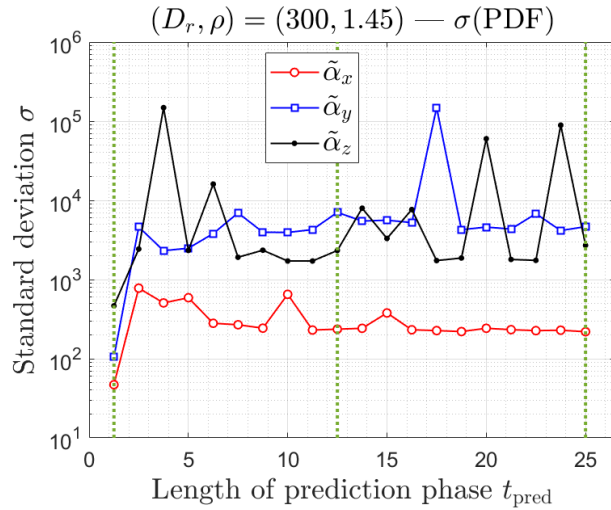


FIG. 10: The evolution in time of the standard deviation σ of the α coefficient PDFs displayed in figure 9 is shown in logarithmic scale for the prediction phase up to $t_{\text{pred}} = 25$. The green dashed vertical lines represent the time windows displayed in figure 9.

with jagged behaviours. Therefore, as already proved by figure 9, the frequency of large value events occur-

ring is higher already after the first time window, but it does not increase additionally in the rest of the prediction phase. However, the standard deviation presents some spikes (especially for $\tilde{\alpha}_y$ and $\tilde{\alpha}_x$), which are symptomatic of a more frequent occurring of the large value events. These large value events, indeed, are correlated with the large error events in the prediction phase, as the relation 10 proves. To conclude, the analysis here performed shows that in the predicted Lorenz system the $\tilde{\alpha}$ coefficients, measured by the PoPe method, are centered around zero. However, quite frequently they differ from the null value, indicating that the actual Lorenz dynamics is definitely impaired. Moreover, the solutions displayed in figure 8 are only representative of the tail of the probability distribution, as the frequency of their occurrence is very low. Hence, even for favorable configurations, the accuracy of such a RC approach must be evaluated cautiously.

IV. DISCUSSION

In this Letter, we have analyzed the validity of the reservoir computing ML technique to predict the trajectories of the Lorenz system, a well-known chaotic system, by the Projection on Proper elements method. Such a method is briefly explained in section II (more details can be found in Refs. [10, 11]). The validity of the RC technique is statistically measured by running $N = 500$ realisations for a large set of configuration parameters. Thus, it has been shown that a good accuracy is achieved only for a small range of (D_r, ρ) configurations of the reservoir. Yet, the error in the prediction phase is significantly increased with respect to the error in the training phase, with a significantly large variation of the error, as figure 3 shows. This implies that quite frequently the RC approach produces predictions strongly affected by large errors of the Lorenz system. It is shown that this is essentially due to the intrinsic randomness of the

RC technique, which inevitably leads to have large error events frequently also for the *favorable* configurations of the network. Additional scans on the relevant parameters of the ML technique such as the length of both training and prediction phases are carried out, showing that the range of validity of this RC approach is even further narrowed. Indeed, a minimum number of time steps in the training phase is required to achieve acceptable results, as figure 7 illustrates, but only for predicting the short-term dynamics of the Lorenz system. The deviation from the exact Lorenz dynamics in the long-term prediction phase is shown to become very large. Such results are also analyzed deeper by means of detailed studies on the time evolution of the Lorenz coefficients computed by the AIS, to determine the validity of the RC approach in this explicit application to the prediction of Lorenz chaotic trajectories. It is shown that the large variation of the Lorenz coefficients computed from the predicted solution can be significant. Therefore, the solution predicted by the AIS based on the RC approach is not necessarily representative of a Lorenz system.

This paper, in the context of the RC approach to the prediction of chaotic time series, is helpful to establish the range of validity of this AIS technique. It also suggests that further developments of the RC paradigm are required in order to robustly achieve a good accuracy in predicting chaotic time series.

ACKNOWLEDGEMENTS

This work has been carried out within the framework of the EUROfusion Consortium and has received funding from the Euratom research and training programme 2014–2018 and 2019–2020 under Grant agreement No 633053. The views and opinions expressed herein do not necessarily reflect those of the European Commission.

-
- [1] Edward N Lorenz. Deterministic nonperiodic flow. *Journal of the atmospheric sciences*, 20(2):130–141, 1963.
 - [2] Jaideep Pathak, Zhixin Lu, Brian R Hunt, Michelle Girvan, and Edward Ott. Using machine learning to replicate chaotic attractors and calculate Lyapunov exponents from data. *Chaos: An Interdisciplinary Journal of Nonlinear Science*, 27(12):121102, 2017.
 - [3] Jaideep Pathak, Brian Hunt, Michelle Girvan, Zhixin Lu, and Edward Ott. Model-free prediction of large spatiotemporally chaotic systems from data: A reservoir computing approach. *Physical review letters*, 120(2):024102, 2018.
 - [4] Mantas Lukoševičius and Herbert Jaeger. Reservoir computing approaches to recurrent neural network training. *Computer Science Review*, 3(3):127–149, 2009.
 - [5] Zhixin Lu, Jaideep Pathak, Brian Hunt, Michelle Girvan, Roger Brockett, and Edward Ott. Reservoir observers: Model-free inference of unmeasured variables in chaotic systems. *Chaos: An Interdisciplinary Journal of Nonlinear Science*, 27(4):041102, 2017.
 - [6] Herbert Jaeger. The “echo state” approach to analysing and training recurrent neural networks. *Bonn, Germany: German National Research Center for Information Technology GMD Technical Report*, 148(34):13, 2001.
 - [7] Wolfgang Maass, Thomas Natschläger, and Henry Markram. Real-time computing without stable states: A new framework for neural computation based on perturbations. *Neural computation*, 14(11):2531–2560, 2002.
 - [8] Ma Qian-Li, Zheng Qi-Lun, Peng Hong, Zhong Tan-Wei, and Qin Jiang-Wei. Multi-step-prediction of chaotic time series based on co-evolutionary recurrent neural network. *Chinese Physics B*, 17(2):536, 2008.
 - [9] Herbert Jaeger and Harald Haas. Harnessing nonlinearity: Predicting chaotic systems and saving energy in wire-

- less communication. *Science*, 304(5667):78–80, 2004.
- [10] Thomas Cartier-Michaud, Philippe Ghendrih, Yanick Sarazin, Jeremie Abiteboul, Hugo Bufferand, Guilhem Dif-Pradalier, Xavier Garbet, Virginie Grandgirard, Guillaume Latu, Claudia Norscini, et al. Projection on proper elements for code control: Verification, numerical convergence, and reduced models. Application to plasma turbulence simulations. *Physics of Plasmas*, 23(2):020702, 2016.
- [11] Thomas Cartier-Michaud, Philippe Ghendrih, Guilhem Dif-Pradalier, Xavier Garbet, Virginie Grandgirard, Guillaume Latu, Yanick Sarazin, Frederic Schwander, and Eric Serre. Verification of turbulent simulations using PoPe: quantifying model precision and numerical error with data mining of simulation output. *Journal of Physics: Conf. Series*, 1125:012005, 2018.
- [12] Paul Erdős and Alfréd Rényi. On random graphs I. *Publicationes Mathematicae Debrecen*, 6:290–297, 1959.
- [13] Edgar N Gilbert. Random graphs. *The Annals of Mathematical Statistics*, 30(4):1141–1144, 1959.